Published in final edited form as:
Biochim Biophys Acta. 2012 November ; 1818(11): 2908–2916. doi:10.1016/j.bbamem.2012.07.009.

Cation Selectivity is a Conserved Feature in the OccD Subfamily of *Pseudomonas aeruginosa*

Jiaming Liu[1], **Aaron J. Wolfe**[2], **Elif Eren**[3], **Jagamya Vijayaraghavan**[3], **Mridhu Indic**[3], **Bert van den Berg**[3], and **Liviu Movileanu**[1,2,4,*]

[1]Department of Physics, Syracuse University, 201 Physics Building, Syracuse, New York 13244-1130, USA

[2]Structural Biology, Biochemistry, and Biophysics Program, Syracuse University, 111 College Place, Syracuse, New York 13244-4100, USA

[3]Program in Molecular Medicine, University of Massachusetts Medical School, Worcester, Massachusetts 01605, USA

[4]Syracuse Biomaterials Institute, Syracuse University, 121 Link Hall, Syracuse, New York 13244, USA

Abstract

To achieve the uptake of small, water-soluble nutrients, *Pseudomonas aeruginosa*, a pathogenic Gram-negative bacterium, employs substrate-specific channels located within its outer membrane (OM). In this paper, we present a detailed description of the single-channel characteristics of six members of the OM carboxylate channel D (OccD) subfamily. Recent structural studies showed that the OccD proteins share common features, such as a closely related, monomeric, 18-stranded β-barrel conformation and large extracellular loops, which are folded back into the channel lumen. Here, we report that the OccD proteins displayed single-channel activity with a unitary conductance covering an unusually broad range, between 20 and 670 pS, as well as a diverse gating dynamics. Interestingly, we found that cation selectivity is a conserved trait among all members of the OccD subfamily, bringing a new distinction between the members of the OccD subfamily and the anion-selective OccK channels. Conserved cation selectivity of the OccD channels is in accord with an increased specificity and selectivity of these proteins for positively charged, carboxylate-containing substrates.

Keywords

Spontaneous gating; Single-molecule biophysics; Single-channel electrical recordings; The OprD family; The OccD subfamily

*Corresponding author: Department of Physics, Syracuse University, 201 Physics Building, Syracuse, New York 13244-1130, USA; Phone: 315-443-8078; Fax: 315-443-9103; lmovilea@physics.syr.edu.

1. Introduction

In many Gram-negative bacteria, such as *Escherichia coli*, the outer membrane (OM) exhibits a high permeability for small water-soluble molecules below a size limit of ~700 Da. This is mainly determined by the presence of non-specific, large-conductance porins, including the OM proteins F (OmpF) [1; 2] and C (OmpC) [3]. In contrast, other Gram-negative bacterial organisms, such as *Pseudomonas aeruginosa*, feature a poor permeability of their OM owing to the absence of highly permeable, large-channel porins. For example, *P. aeruginosa* displayed between 12- to 100-fold lower outer membrane permeability for a variety of small nutrients as compared to *E. coli* [4]. This is the fundamental reason for the intrinsic resistance of this bacterium to antibiotics and antimicrobials. Instead, such organisms efficiently take up a broad range of small, polar and nonpolar substrates through the members of the outer membrane carboxylate channel (Occ) family, formerly called OprD family [4–6]. In *P. aeruginosa*, the Occ family of specific channels comprises 19 members, which mediate the uptake of small nutrients for the growth and vitality of the cell. Although these OM proteins showed an unusual amino acid sequence similarity (46–57%) [7; 8] (Supplementary Materials, Fig. S1), they displayed a broad diversity among substrate specificity and selectivity [9]. In the last decade, phylogenetic analysis of the Occ family indicated that they fall into two distinct clusters, each of which bearing similarity to either OccD or OccK proteins [8]. The OccD subfamily includes 8 members, whereas the OccK subfamily includes 11 members [7; 8].

In the last few years, the X-ray crystal structures of nine Occ channels were obtained [10–12], prompting functional studies of these OM proteins [9; 12–14]. The OccD1 protein, which was formerly called OprD, represents the prototype of the substrate-specific OccD subfamily. Its crystal structure reveals a monomeric 18-stranded β-barrel with large extracellular loops, such as L3, L4 and L7, folded back into the channel lumen [10]. The channel interior is characterized by a central constriction with a polarized distribution of charged residues: positively charged amino acids are located on one side and an electronegative cluster of residues on the other side. Previously, Trias and Nikaido (1990) [15] and Huang and Hancock (2003) [16] determined that the lumen of the OccD1 protein channel from *P. aeruginosa* contains a binding site for basic residues and short cationic peptides. In accord with these prior results, van den Berg and co-workers confirmed that OccD1 has a preference for arginine and other basic amino acids as substrates [9]. Moreover, OccD1 was found to be an imipemen-specific channel [16–18]. The recently obtained crystal structures of OccD2 and OccD3, which were formerly called OpdC and OpdP, respectively, indicated a similar monomeric structure of these OM proteins, as compared to OccD1 (Fig. 1).

In this paper, we report a systematical single-channel electrical analysis of the six members (out of a total of eight members) of the OccD subfamily that could be overexpressed and purified. The proteins inspected in this work were OccD1, OccD2, OccD3, OccD4 (formerly OpdT), OccD5 (OpdI) and OccD6 (OprQ). Among these channels, OccD4, OccD5 and OccD6 do not have an available X-ray crystal structure. Using single-channel reconstitution on planar lipid bilayers under similar experimental circumstances, we determined that their unitary conductance falls in a much broader range than earlier expectations. For example, we confirmed that OccD1 and OccD5 display a low-conductance channel signature, with a unitary conductance of ~20 pS, but OccD3 showed a robust large single-channel conductance of ~670 pS. Moreover, OccD6 exhibited an unusually high conductance with two major open sub-states of ~420 and ~1900 pS. Employing reversal potential determinations under asymmetric ion concentration conditions, we demonstrate that that all members of the OccD subfamily are cation selective, which is in accord with the recent *in vitro* transport assays showing specificity and selectivity of these OM proteins for positively

charged, carboxylate-containing substrates [9; 15; 16]. This results contrast to the recent determinations of anion selectivity with all members of the OccK subfamily. Therefore, ion selectivity assay established additional distinctions between the members of the OccD and OccK subfamilies.

2. Materials and Methods

2.1. Cloning, expression, and purification of the OccD proteins

Signal sequence cleavage sites of OccD proteins were predicted with Signal P 4.0 (http://www.cbs.dtu.dk/services/SignalP/), after which the mature parts of the *occd* genes from *P. aeruginosa* were amplified by PCR from genomic DNA and cloned into the *E. coli* expression vector pB22 [19; 20], having the signal sequence of the *E. coli* OM protein YtfM and an N-terminal hepta-histidine tag for purification. BL21(DE3) T1 phage-resistant cells (New England Biolabs, Ipswich, MA) were transformed with pB22-OccD constructs. The cells were grown to OD600 ~ 0.5–1.0 at 37°C (dependent on the protein), induced with 0.1% arabinose at 20°C overnight or at 30°C for 4–6 hrs. Other details of the standard protein chemistry protocols used in this work were published previously [12; 13]. The purity of the OccD protein samples was assessed by SDS-PAGE gel electrophoresis.

2.2. Single-channel current recordings on planar lipid bilayers

Single-channel current measurements were carried out with planar lipid membranes [21; 22]. The standard electrolyte in both chambers was 1 M KCl, 10 mM potassium phosphate, pH 7.4, unless otherwise stated. The bilayer was formed with 1,2-diphytanoyl-*sn*-glycerophosphocholine (Avanti Polar Lipids Inc., Alabaster, AL, USA). OccD proteins were added to the *cis* chamber, which was grounded. A positive current is defined such that it represents a positive charge moving from the *trans* to *cis* chamber. Currents were recorded by using an Axopatch 200B patch-clamp amplifier (Axon Instruments, Foster City, CA) connected to the chambers by Ag/AgCl electrodes. An Optiplex Desktop Computer (Dell, Austin, TX) equipped with a Digitdata 1440 A/D converter (Axon) was used for data acquisition. Acquisition and analysis of single-channel data were performed using pClamp 10.2 software (Axon). We used protein samples from one or more purification batches and discovered satisfactory reproducibility of the single-channel electrical signatures [9–13].

3. Results

3.1. OccD proteins exhibit multistate, single-channel dynamics

We conducted most of our single-channel electrical recordings in 1 M KCl, 10 mM potassium phosphate, pH 7.4. These conditions were motivated by the very small diameter of the central constriction within the channel lumen of the OccD proteins (Fig. 1), revealing a small pore. Indeed, we determined that the OccD1 protein, the archetype of the OccD subfamily, forms a low-conductance channel in planar lipid bilayers, confirming previously carried out electrophysiological work from different groups [10; 23; 24]. Here, we define a low-, medium- and large-conductance channel as an OM protein whose single-channel conductance of the most probable open sub-state is in the range 0–100, 100–500 and 500–1000 pS, respectively. The unitary conductance of OccD1 is 21 ± 3 pS (Fig. 2A, Table 1). The single-channel electrical signature of the OccD1 channel reveals a most probable open sub-state O_1, which is stable for lengthy periods, in the range of hours, but decorated by short-lived, infrequent and large-amplitude current spikes with an average conductance of 889 ± 102 pS (the O_2 open sub-state). The duration of these current spikes underwent a Poisson distribution with a single exponential of the probability function (Fig. 3A). The dwell time of the upward current spikes of the OccD1 channel, extracted from a typical single-channel experiment, was $\tau_{O2} = 0.11 \pm 0.02$ ms.

The average dwell times were derived from standard event duration histograms of the single-channel electrical data. The fits of the data were achieved employing log likelihood ratio (LLR) tests to compare various fitting models [25–27]. We determined that the fit of the dwell time histograms contained a well-defined single- or two-exponential distribution function. Fits to a three-exponential distribution or stretched exponentials were not statistically better than single- or two-exponentials models, as judged by the LLR value at a confidence level of 0.95. A closely similar single-channel electrical signature to OccD1 was found with the OccD2 channel (Fig. 2B). However, this channel showed some variability of the baseline of the O_1 sub-state from experiment to experiment and from batch to batch. For example, the single-channel current corresponding to the O_1 open sub-state varied between 2 and 17 pA at an applied transmembrane potential of +60 mV. Based upon these experiments, we judge that its single-channel conductance is in the range of several tens of pS, which is consistent with a low-conductance protein channel.

In contrast to the results obtained with OccD1 and OccD2, the single-channel electrical signature of the OccD3 protein revealed a large-conductance channel with a unitary conductance of 677 ± 71 pS, corresponding to the most probable O_2 open sub-state (Fig. 2C, Table 1). This channel experienced downward, large amplitude current blockades to the zero-conductance O_1 open sub-state, with a dwell time showing a two-exponential probability function ($\tau_{O1\text{-}1}$ = 06 ± 0.01 ms and $\tau_{O1\text{-}2}$ = 0.92 ± 0.04 ms with the event probabilities $P_{O1\text{-}1}$ = 0.51 ± 0.06 and $P_{O1\text{-}2}$ = 0.49 ± 0.01; Fig. 3B). The OccD4 exhibited a medium-conductance channel signature with a unitary conductance of 158 ± 8 pS that corresponds to the most probable O_2 open sub-state (Fig. 2D). Its single-channel electrical signature featured very short-lived, highly frequent and low-amplitude current spikes that were not time-resolvable. Another example of a low-conductance OccD channel that is similar to OccD1 is OccD5 (Fig. 2E). This channel has a unitary conductance of 24 ± 11 pS, which is closely similar to OccD1 (Fig. 2A and Table 1). However, the upward current spikes observed with OccD5, at the O_2 open sub-state, showed a much longer dwell time, in the range of several milliseconds, as compared to compared to OccD1. A representative single-channel experiment demonstrated that the dwell time of the O_2 events followed a two-exponential probability function distribution with $\tau_{O2\text{-}1}$ = 4.2 ± 0.3 ms, $\tau_{O2\text{-}2}$ = 15.3 ± 0.7 ms and with the event probabilities $P_{O2\text{-}1}$ = 0.44 ± 0.10 and $P_{O2\text{-}2}$ = 0.56 ± 0.01, respectively (Fig. 3C).

Surprisingly, the OccD6 channel displayed a dynamic single-channel electrical signature with two major, open sub-states, O_1 and O_2 (Fig. 2F). These sub-states showed a conductance of 417 ± 117 pS and 1889 ± 151 pS, respectively. The brief closures to the O_1 open sub-state had a dwell time with two components $\tau_{O1\text{-}1}$ = 0.12 ± 0.01 ms and $\tau_{O1\text{-}2}$ = 1.9 ± 0.2 ms with the event probabilities $P_{O1\text{-}1}$ 0.41 ± 0.01 and $P_{O1\text{-}2}$ = 0.59 ± 0.04, respectively (Fig 3D). The duration of the O_2 events were characterized by $\tau_{O2\text{-}1}$ = 4.6 ± 0.5 ms and $\tau_{O2\text{-}2}$ = 81.5 ms ± 3.8 ms (Fig. 3E). These single-channel events displayed the probabilities of $P_{O2\text{-}1}$ = 0.53 ± 0.02 and $P_{O2\text{-}2}$ = 0.47 ± 0.02, respectively. OccD6 fluctuated between these major open sub-states. Based upon long durations of the overall O_2 sub-state, we consider that this is another large-conductance OccD channel, in addition to OccD3, which is quite distinct from other members of the OccD and OccK subfamilies [12].

3.2. Voltage dependence of the unitary conductance of the OccD proteins

We also inspected whether the ion conduction thorough the OccD channels follows an Ohmic behavior. Therefore, the current-voltage relationships for the open sub-states observed with the OccD proteins are illustrated in Fig. 4. In most panels, the range of the applied transmembrane potential was −80 to +80 mV, because at voltages greater than these values some OccD channels became unstable. Furthermore, we calculated the asymmetry conductance ratio of the most probable open sub-state (g_{80}/g_{-80}) as the ratio between the

unitary conductance measured at +80 mV and the unitary conductance measured at −80 mV (Table 1). This value is close to unity for channels featuring fairly Ohmic conduction. For example, OccD2, OccD4 and OccD6 exhibited Ohmic conduction profiles with asymmetry conductance ratios of 0.99 ± 0.33, 1.11 ± 0.08 and 0.99 ± 0.16, respectively. In contrast, OccD1, OccD3 and OccD5 displayed non-Ohmic conduction profiles with asymmetry conductance ratios of 2.58 ± 0.97, 2.55 ± 0.26 and 0.42 ± 0.08, respectively.

3.3. Kinetics of the current transitions in the OccD3 channel

We examined the details of the two-state current transitions observed with the OccD3 channel. The crystal structure of the OccD3 channel reveals an open pore with a very narrow central constriction, which measures ~3.5 Å in diameter (Fig. 1 and Table 2). Despite its very small eyelet, the unitary conductance of the most probable open sub-state O_1 of the OccD3 channel was ~670 pS (Table 1), which is pertinent to a large-conductance transmembrane protein. This value is comparable to the single-channel conductance measured with the trimeric OmpF, which is ~700 pS per monomer in 1 M KCl [28; 29]. The unitary conductance of the OmpC is ~900 pS per monomer in 1 M KCl [30]. The kinetic rate constants of the O_1 and O_2 open sub-states were determined using the reciprocal of the mean lifetime, which was extracted from fits of the standard dwell-time histograms [26]:

$$k_{O1\rightarrow O2}=\frac{1}{\tau_{O1}} \quad (1)$$

$$k_{O2\rightarrow O1}=\frac{1}{\tau_{O2}} \quad (2)$$

where τ_{O1} and τ_{O2} are the mean lifetimes of the O_1 and O_2 open sub-states, respectively. The mean lifetime was determined using the event probability and the dwell time extracted from histograms, as follows:

$$\tau_{O1}=P_{O1-1}\tau_{O1-1}+P_{O1-2}\tau_{O1-2} \quad (3)$$

$$\tau_{O2}=P_{O2-1}\tau_{O2-1}+P_{O2-2}\tau_{O2-2} \quad (4)$$

Because the O_2 open sub-state is the most probable, the $k_{O1\rightarrow O2}$ kinetic rate constant is greater than the $k_{O2\rightarrow O1}$ kinetic rate constant.

Voltage dependence of the rate constants of the OccD3 channel is displayed in Fig. 5A. While $k_{O1\rightarrow O2}$ is voltage independent, $k_{O2\rightarrow O1}$ decreased by increasing the applied transmembrane potential from −80 to +80 mV, meaning that the event frequency of the large-amplitude current blockades decreased at more positive voltages. Based upon this observation, we constructed the voltage-dependent model of the two open sub-state, free energy landscape of the large-conductance OccD3 protein channel (Fig. 5B). In a very simplistic representation, this landscape features two activation free energies: the small, voltage-independent $\Delta G^{\neq}_{O1\rightarrow O2}$ barrier and the large, voltage-dependent $\Delta G^{\neq}_{O1\rightarrow O2}$ barrier. This data suggests that the large-amplitude current blockades of the OccD3 channel might be likely produced by a positively charged plug of the pore lumen in the form of an extracellular loop or the N-terminal part of the protein (Fig. 1C). For example, the X-ray crystal structure of the OccD3 protein revealed that the 30-residue long, N-terminal part projects within the channel lumen from the *cis* side, making a substantial contribution to the narrow-diameter central constriction.

3.4. OccD proteins form cation-selective channels

We examined the preferential ionic permeability of the OccD channels for cations versus anions using the permeability ratio (P_K/P_{Cl}). The salt gradient assay was used to infer the reversal potential (V_r). The calculation of the permeability ratio was accomplished using the Goldman–Hodgkin–Katz formalism [31; 32]:

$$\frac{P_K}{P_{Cl}} = \frac{[a_{Cl^-}]_t - [a_{Cl^-}]_c e^{VrF/RT}}{[a_{K^+}]_t e^{VrF/RT} - [a_{K^+}]_c} \quad (5)$$

where the variable *a* represents the activity of either potassium or chloride in either the *cis* (subscript "*c*") or *trans* (subscript "*t*") chamber. Here, F, R and *T* are the Faraday constant, the gas constant and the absolute temperature, respectively. The x-axis intercept of the I–V curve is the desired reversal potential, which was used to offset the resting potential, making the current zero. In Table 1, we present the reversal potential V_r and the calculated P_K/P_{Cl} (eqn. (5)). Here, we define a weakly cation-selective, a cation-selective and a strongly cation-selective channel as an OM protein whose permeability ratio P_K/P_{Cl} is in the range 1–5, 5–10 and 10–100, respectively. The OccD1 channel exhibited a weak cation selectivity with a permeability ratio of 2.5 ± 1.0. Weak cation selectivity was also observed with OccD2, OccD3 and OccD4. In contrast, OccD6 displayed a cation selectivity of 5.0 ± 1.4. OccD5 showed a high cation selectivity with a permeability ratio P_K/P_{Cl} of 12 ± 4.

4. Discussion

In this paper, we show a systematical single-channel analysis of the six members of the OccD subfamily. We were surprised to discover quite a broad range of unitary conductance of the OccD channels, contradicting with the hypothesis that the OM of *P. aeruginosa* lacks large-conductance protein channels. The single-channel conductance of OccD1, the archetype of the OccD subfamily, is 21 ± 3 pS, in accord with the previous single-channel measurements [10; 23; 24]. This very small conductance is consistent with the recent X-ray crystal structure of this protein, which indicates a very small central eyelet [9; 10]. One question regards the presence of brief, upwards, large-amplitude current spikes, which were observed in the case of electrical recordings with the OccD channels. For instance, OccD1 showed a most probable open sub-state with a low conductance (21 ± 3) decorated by current fluctuations to an open sub-state with a much greater conductance (889 ± 102 pS). We are certain that the upwards current fluctuations are not caused by the type of used buffer. For example, they were also noticed in single-channel recordings with OccD1 reconstituted in 1 M NaCl, 2.5 mM 2 (N-morpholino)ethane sulfonic acid (MES)-NaOH buffer, pH 5.9 at an applied transmembrane potential of 100 mV [23]. In the past, single-channel reconstitutions with a loop-deletion mutant, OccD1-ΔL3, resulted in a substantially increased unitary conductance (~90 pS) [10], confirming that loop L3 is indeed one of the large extracellular loops folded back into the channel lumen and is part of the central constriction. Single-channel current fluctuations observed with the members of the OccD sub-family indirectly confirm the presence of flexible and large extracellular loops that are folded back into the channel lumen. Such current fluctuations were also observed with other β-barrel membrane proteins [33–40].

The single-channel conductance of the OccD1 was much smaller than that recorded with OccK1 (~240 pS), which is the archetype of the OccK subfamily [11]. The measurements of the single-channel conductance of OccD1 and OccK1 are in agreement with their high-resolution X-ray crystal structure [9], which indicates a wider central constriction of OccK1 than that of OccD1 [12]. The structures of OccD1, OccD2 and OccD3 show a very narrow constriction of the channel lumen with diameters smaller than 4 Å (Table 2). Crystal

structures and sequence alignment of the members of the OccD subfamily revealed that the residues lining the central constriction are not conserved [9; 10]. Therefore, some distinctions in the unitary conductance and gating dynamics among the OccD protein channels were anticipated.

In contrast to the results obtained with OccD1 and OccD5, which showed low conductance, OccD3 displayed a robust single-channel electrical signature with a large unitary conductance of 667 ± 71 pS, but accompanied by downward current spikes, many of which had a complete channel block (Supplementary Materials, Fig. S2). Taking into consideration the very narrow constriction of the OccD3 channel (Table 2) [9], its crystal structure does not seem to represent the most probable open sub-state. This finding suggests that the folding and local flexibility of the extracellular loops might be different when the protein is reconstituted into a planar bilayer from those under crystallization conditions [9]. More experimentation and computational work is needed to obtain a clarification on the discrepancies between the X-ray crystal structure information and single-channel electrical data (see below). It is also conceivable that the local flexibility and dynamics, the number of charges as well as the position of the individual large extracellular loops along the longitudinal axis of the lumen affect the unitary conductance of the OccD protein under inspection. The positions of the local charges within or near the central eyelet are essential for both the ion selectivity of the protein and the unitary conductance. We determined that the OccD3 protein features a cluster of four negatively charged residues within the constriction (D11, E18, D171 and D342). We hypothesize that these residues make a network of acidic charges that result in a cation selectivity of the OccD3 channel (Table 1, Table 2). However, we were not able to determine a clear, distinct contribution of the negative charges within the lumen of the OccD1 and OccD2 proteins due to the non-uniform and corrugated surface within their constriction.

Under these conditions, is the large-conductance open sub-state of OccD3 physiologically significant? If so, what is its meaning? If the channel mediates the translocation of a molecule, that process requires the opening of the protein, which might result in a large-conductance open sub-state. Regardless, the lipid composition of our bilayer membranes as well as the lack of bacterial lipopolysaccharides (LPS) of *P. aeruginosa* might significantly contribute to the deviations of the single-channel electrical signature from those presented in this paper. Previously, Ishii and Nakae (1993) demonstrated that LPS promote the opening of the OccD1 channel [23]. This protein formed low-conductance channels in LPS-free lipid bilayers (~30 pS), but displayed rapid large-current amplitude opening events, with a conductance of ~400 pS, in LPS-containing lipid bilayers. The duration of closing events was longer at very low applied transmembrane potentials.

How do the single-channel electrical signatures of the OccD channels compare and contrast with those recorded with the OccK channels? Recent channel reconstitution studies also confirmed the diversity of single-channel signatures among the OccK channels [12]. The members of the OccK subfamily exhibited distinct unitary conductance values, which fall into two clusters: the low- (40–100 pS) and medium (100 – 500 pS) - conductance protein channels. Large-amplitude current fluctuations decorating an open substate were noticed with OccK1, OccK2, OccK4, OccK5, OccK6 and OccK7. In this work, we show that OccD6 has two major, large-conductance, open sub-states, O_1 and O_2. Given the poor permeability of the OM of *P. aeruginosa*, this finding was very surprising. It might be possible that the major large-conductance open sub-state (O_2) observed in single-channel recordings with OccD6 is not noticeable under physiological conditions and other circumstances of the OM of *P. aeruginosa*.

In this paper, we established that all investigated members of the OccD subfamily are cation-selective OM proteins. OccD1, OccD2, OccD3 and OccD4 showed modest selectivity, whereas increased permeability ratios of cations versus anions were noticed for the OccD5 and OccD6 channels. Cation selectivity among the members of the OccD subfamily is in agreement with their increased selectivity and specificity for positively charged substrates [9]. For example, OccD1 was found to facilitate the transport of positively charged residues and short di- and tri- peptides containing them [15]. Very recently, Eren and co-workers, using *in vitro* transport assays, determined that the members of OccK subfamily are good transporters for the negatively charged benzoate and pyroglutamate, in accord with their anion selectivity features determined from systematical single-channel analysis [9; 12]. In contrast, all OccD channels, with some exception for OccD4, were good transporters for arginine, a basic residue, which is in accord with the cation-selectivity results determined in this work [9]. The transport performance for arginine, which was measured through the specific substrate uptake was not well correlated with the measured values of ion selectivity, indicating that the transport efficiency is a complex function not only depending on ion selectivity, but likely on the structure of the channel lumen and the properties of the substrate as well. For example, OccD1 and OccD3, although they featured poor cation selectivity, displayed the highest specific uptakes for arginine.

The availability of structural, biochemical and biophysical information on the members of the OccD subfamily will ignite immediate theoretical and computational studies for a better mechanistic and quantitative understanding of the transport of small water-soluble molecules across these OM proteins in *P. aeruginosa*. Full-atomistic molecular dynamics (MD) simulations might be used in the future to unravel the mechanistic details of the stochastic motions of the extracellular loops, which are folded back into the channel lumen. Only a fraction of the motions of the large loops are observed in the single-channel electrical recordings owing to limited time resolution of the employed instrumentation [41; 42]. Molecular modelers might be able to infer critical information regarding the flexibility and dynamics of individual loops of the members of the OccD subfamily [43–48].

Needless to say that the environmental conditions, such as applied transmembrane potential, temperature, lipid composition of the bilayer, pH, ionic strength of the aqueous phase as well as osmotic stress of the co-solutes can impact the dynamics and local flexibility of the extracellular loops. For instance, it was found that the conformations of the extracellular loops of the OM protein OpcA from *Neisseria meningitides* are affected by both the ionic strength of the aqueous phase and the lipid bilayer environment [45]. Therefore, it is not surprising to find distinctions between the information obtained from X-ray crystal structure and high-resolution single-channel electrical recordings. One example pertinent to this work is the large-conductance open sub-state of the OccD3 protein. This finding is in disagreement with its X-ray structure, which shows a narrow constriction smaller than 4 Å (Fig. 1, Table 2). The mechanism of this disagreement between the two approaches is not clear, which would be the reason for a particularly attractive theme for a systematical MD study. Finally, the availability of the structure of three OccD proteins along with comprehensive single-channel electrical data of six OccD proteins will represent a solid platform for determining the molecular basis of their conserved cation selectivity.

Supplementary Material

Refer to Web version on PubMed Central for supplementary material.

Acknowledgments

We are grateful to all colleagues in the Movileanu and van den Berg research groups, who provided technical assistance at various stages of this work. This paper was funded in part by grants from the US National Science Foundation (DMR-1006332, L.M.) and the National Institutes of Health (R01 GM088403, L.M. and R01 GM085785, B.v.d.B).

ABBREVIATIONS AND SYMBOLS

LPS	Lipopolysaccharide
OM	Outer membrane of Gram-negative bacterium
Occ	Outer membrane carboxylate channel family of *P. aeruginosa*
OccD	Outer membrane carboxylate channel D subfamily of *P. aeruginosa*
OccK	Outer membrane carboxylate channel K subfamily of *P. aeruginosa*
OmpC	Outer membrane protein C of *E. coli*
OmpF	Outer membrane protein F of *E. coli*

Reference List

1. Cowan SW, Garavito RM, Jansonius JN, Jenkins JA, Karlsson R, Konig N, Pai EF, Pauptit RA, Rizkallah PJ, Rosenbusch JP. The structure of OmpF porin in a tetragonal crystal form. Structure. 1995; 3:1041–1050. [PubMed: 8589999]
2. Yamashita E, Zhalnina MV, Zakharov SD, Sharma O, Cramer WA. Crystal structures of the OmpF porin: function in a colicin translocon. EMBO J. 2008; 27:2171–2180. [PubMed: 18636093]
3. Basle A, Rummel G, Storici P, Rosenbusch JP, Schirmer T. Crystal structure of osmoporin OmpC from E. coli at 2.0 A. J Mol Biol. 2006; 362:933–942. [PubMed: 16949612]
4. Hancock RE, Brinkman FS. Function of pseudomonas porins in uptake and efflux. Annu Rev Microbiol. 2002; 56:17–38. [PubMed: 12142471]
5. Nikaido H. Molecular basis of bacterial outer membrane permeability revisited. Microbiol Mol Biol Rev. 2003; 67:593–656. [PubMed: 14665678]
6. Hancock, REW.; Tamber, S. Porins of the Outer Membrane of Pseudomonas aeruginosa. In: Benz, R., editor. Bacterial and Eukaryotic Porins: Structure, Function, Mechanism. Wiley-VCH; Weinheim: 2004. p. 61-77.
7. Tamber S, Hancock RE. Involvement of two related porins, OprD and OpdP, in the uptake of arginine by Pseudomonas aeruginosa. FEMS Microbiol Lett. 2006; 260:23–29. [PubMed: 16790014]
8. Tamber S, Ochs MM, Hancock RE. Role of the novel OprD family of porins in nutrient uptake in Pseudomonas aeruginosa. J Bacteriol. 2006; 188:45–54. [PubMed: 16352820]
9. Eren E, Vijayaraghavan J, Liu J, Cheneke BR, Touw DS, Lepore BW, Indic M, Movileanu L, van den Berg B. Substrate specificity within a family of outer membrane carboxylate channels. PLoS Biology. 2012; 10:e1001242. [PubMed: 22272184]
10. Biswas S, Mohammad MM, Patel DR, Movileanu L, van den Berg B. Structural insight into OprD substrate specificity. Nat Struct Mol Biol. 2007; 14:1108–1109. [PubMed: 17952093]
11. Biswas S, Mohammad MM, Movileanu L, van den Berg B. Crystal structure of the outer membrane protein OpdK from Pseudomonas aeruginosa. Structure. 2008; 16:1027–1035. [PubMed: 18611376]
12. Liu J, Eren E, Vijayaraghavan J, Cheneke BR, Indic M, van den Berg B, Movileanu L. OccK Channels from Pseudomonas aeruginosa Exhibit Diverse Single-channel Electrical Signatures, but Conserved Anion Selectivity. Biochemistry. 2012; 51:2319–2330. [PubMed: 22369314]
13. Cheneke BR, van den Berg B, Movileanu L. Analysis of gating transitions among the three major open states of the OpdK channel. Biochemistry. 2011; 50:4987–4997. [PubMed: 21548584]

14. Cheneke BR, Indic M, van den Berg B, Movileanu L. An Outer Membrane Protein undergoes Enthalpy- and Entropy-driven Transitions. Biochemistry. 2012; 51:5348–5358.
15. Trias J, Nikaido H. Protein D2 channel of the Pseudomonas aeruginosa outer membrane has a binding site for basic amino acids and peptides. J Biol Chem. 1990; 265:15680–15684. [PubMed: 2118530]
16. Huang H, Hancock RE. Genetic definition of the substrate selectivity of outer membrane porin protein OprD of Pseudomonas aeruginosa. J Bacteriol. 1993; 175:7793–7800. [PubMed: 8253668]
17. Huang H, Hancock RE. The role of specific surface loop regions in determining the function of the imipenem-specific pore protein OprD of Pseudomonas aeruginosa. J Bacteriol. 1996; 178:3085–3090. [PubMed: 8655484]
18. Ochs MM, Bains M, Hancock RE. Role of putative loops 2 and 3 in imipenem passage through the specific porin OprD of Pseudomonas aeruginosa. Antimicrob Agents Chemother. 2000; 44:1983–1985. [PubMed: 10858367]
19. Guzman LM, Belin D, Carson MJ, Beckwith J. Tight regulation, modulation, and high-level expression by vectors containing the arabinose PBAD promotor. J Bacteriol. 1995; 177:4121–4130. [PubMed: 7608087]
20. van den BB, Clemons WM Jr, Collinson I, Modis Y, Hartmann E, Harrison SC, Rapoport TA. X-ray structure of a protein-conducting channel. Nature. 2004; 427:36–44. [PubMed: 14661030]
21. Goodrich CP, Kirmizialtin S, Huyghues-Despointes BM, Zhu AP, Scholtz JM, Makarov DE, Movileanu L. Single-molecule electrophoresis of beta-hairpin peptides by electrical recordings and Langevin dynamics simulations. J Phys Chem B. 2007; 111:3332–3335. [PubMed: 17388500]
22. Mohammad MM, Prakash S, Matouschek A, Movileanu L. Controlling a single protein in a nanopore through electrostatic traps. J Am Chem Soc. 2008; 130:4081–4088. [PubMed: 18321107]
23. Ishii J, Nakae T. Lipopolysaccharide promoted opening of the porin channel. FEBS Lett. 1993; 320:251–255. [PubMed: 8385028]
24. Ishii J, Nakae T. Specific interaction of the protein-D2 porin of Pseudomonas aeruginosa with antibiotics. FEMS Microbiol Lett. 1996; 136:85–90. [PubMed: 8919460]
25. McManus OB, Blatz AL, Magleby KL. Sampling, Log Binning, Fitting, and Plotting Durations of Open and Shut Intervals From Single Channels and the Effects of Noise. Pflugers Arch. 1987; 410:530–553. [PubMed: 2448743]
26. Bikwemu R, Wolfe AJ, Xing X, Movileanu L. Facilitated translocation of polypeptides through a single nanopore. J Phys Condens Matter. 2010; 22:454117. [PubMed: 21339604]
27. Niedzwiecki DJ, Grazul J, Movileanu L. Single-molecule observation of protein adsoption onto an inorganic surface. J Am Chem Soc. 2010; 132:10816–10822. [PubMed: 20681715]
28. Saint N, Lou KL, Widmer C, Luckey M, Schirmer T, Rosenbusch JP. Structural and functional characterization of OmpF porin mutants selected for larger pore size. II. Functional characterization. J Biol Chem. 1996; 271:20676–20680. [PubMed: 8702817]
29. Chimerel C, Movileanu L, Pezeshki S, Winterhalter M, Kleinekathofer U. Transport at the nanoscale: Temperature dependance of ion conductance. Eur Biophys J. 2008; 38:121–125. [PubMed: 18726094]
30. Biro I, Pezeshki S, Weingart H, Winterhalter M, Kleinekathofer U. Comparing the temperature-dependent conductance of the two structurally similar E. coli porins. OmpC and OmpF Biophys J. 2010; 98:1830–1839.
31. Hille, B. Ion Channels of Excitable Membranes. Sinauer Associates, Inc; Sunderland, Massachusetts, USA: 2001.
32. Wolfe AJ, Mohammad MM, Cheley S, Bayley H, Movileanu L. Catalyzing the translocation of polypeptides through attractive interactions. J Am Chem Soc. 2007; 129:14034–14041. [PubMed: 17949000]
33. Liu N, Delcour AH. The spontaneous gating activity of OmpC porin is affected by mutations of a putative hydrogen bond network or of a salt bridge between the L3 loop and the barrel. Protein Eng. 1998; 11:797–802. [PubMed: 9796829]

34. Liu N, Samartzidou H, Lee KW, Briggs JM, Delcour AH. Effects of pore mutations and permeant ion concentration on the spontaneous gating activity of OmpC porin. Protein Eng. 2000; 13:491–500. [PubMed: 10906344]
35. Basle A, Iyer R, Delcour AH. Subconductance states in OmpF gating. Biochim Biophys Acta. 2004; 1664:100–107. [PubMed: 15238263]
36. Jung Y, Bayley H, Movileanu L. Temperature-responsive protein pores. J Am Chem Soc. 2006; 128:15332–15340. [PubMed: 17117886]
37. Jung YH, Cheley S, Braha O, Bayley H. The internal cavity of the staphylococcal α-hemolysin pore accommodates ~175 exogenous amino acid residues. Biochemistry. 2005; 44:8919–8929. [PubMed: 15966717]
38. Mapingire OS, Henderson NS, Duret G, Thanassi DG, Delcour AH. Modulating effects of the plug, helix, and N- and C-terminal domains on channel properties of the PapC usher. J Biol Chem. 2009; 284:36324–36333. [PubMed: 19850919]
39. Mohammad MM, Howard KR, Movileanu L. Redesign of a plugged beta-barrel membrane protein. J Biol Chem. 2011; 286:8000–8013. [PubMed: 21189254]
40. Mohammad MM, Iyer R, Howard KR, McPike MP, Borer PN, Movileanu L. Engineering a Rigid Protein Tunnel for Biomolecular Detection. J Am Chem Soc. 2012; 134:9521–9531. [PubMed: 22577864]
41. Sackmann, B.; Neher, E. Single-Channel Recording. Kluwer Academic/Plenum Publishers; New York: 1995.
42. Movileanu L, Cheley S, Bayley H. Partitioning of individual flexible polymers into a nanoscopic protein pore. Biophys J. 2003; 85:897–910. [PubMed: 12885637]
43. Faraldo-Gomez JD, Smith GR, Sansom MS. Setting up and optimization of membrane protein simulations. Eur Biophys J. 2002; 31:217–227. [PubMed: 12029334]
44. Faraldo-Gomez JD, Smith GR, Sansom MS. Molecular dynamics simulations of the bacterial outer membrane protein FhuA: a comparative study of the ferrichrome-free and bound states. Biophys J. 2003; 85:1406–1420. [PubMed: 12944258]
45. Bond PJ, Derrick JP, Sansom MS. Membrane simulations of OpcA: gating in the loops? Biophys J. 2007; 92:L23–L25. [PubMed: 17114231]
46. Luan B, Caffrey M, Aksimentiev A. Structure refinement of the OpcA adhesin using molecular dynamics. Biophys J. 2007; 93:3058–3069. [PubMed: 17938421]
47. Maffeo C, Aksimentiev A. Structure, dynamics, and ion conductance of the phospholamban pentamer. Biophys J. 2009; 96:4853–4865. [PubMed: 19527644]
48. Luan B, Carr R, Caffrey M, Aksimentiev A. The effect of calcium on the conformation of cobalamin transporter BtuB. Proteins. 2010; 78:1153–1162. [PubMed: 19927326]
49. Mohammad MM, Movileanu L. Impact of distant charge reversals within a robust beta-barrel protein pore. J Phys Chem B. 2010; 114:8750–8759. [PubMed: 20540583]
50. Smart OS, Neduvelil JG, Wang X, Wallace BA, Sansom MS. HOLE: a program for the analysis of the pore dimensions of ion channel structural models. J Mol Graph. 1996; 14:354–60. 376. [PubMed: 9195488]
51. Smart OS, Coates GM, Sansom MS, Alder GM, Bashford CL. Structure-based prediction of the conductance properties of ion channels. Faraday Discuss. 1998:185–199. [PubMed: 10822609]
52. Smart OS, Breed J, Smith GR, Sansom MS. A novel method for structure-based prediction of ion channel conductance properties. Biophys J. 1997; 72:1109–1126. [PubMed: 9138559]
53. Pettersen EF, Goddard TD, Huang CC, Couch GS, Greenblatt DM, Meng EC, Ferrin TE. UCSF Chimera--a visualization system for exploratory research and analysis. J Comput Chem. 2004; 25:1605–1612. [PubMed: 15264254]
54. McManus OB, Magleby KL. Kinetic states and modes of single large-conductance calcium-activated potassium channels in cultured rat skeletal-muscle. J Physiol(Lond). 1988; 402:79–120. [PubMed: 3236256]
55. Mohammad MM, Movileanu L. Excursion of a single polypeptide into a protein pore: simple physics, but complicated biology. Eur Biophys J. 2008; 37:913–925. [PubMed: 18368402]

Highlights

- We present detailed single-channel features of six members of the OccD subfamily.
- OccD proteins displayed a unitary conductance covering a broad range
- Cation selectivity is a conserved trait among the members of the OccD subfamily

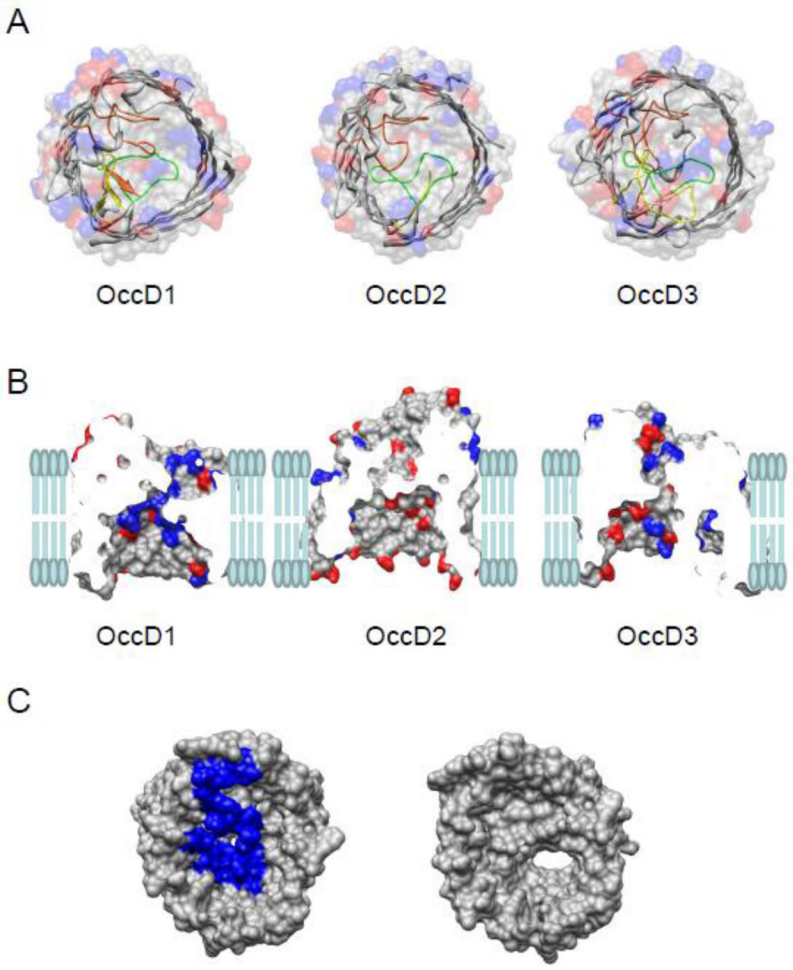

Figure 1. Structural representation of OccD subfamily protein channels

(**A**) Molecular surface and ribbon representations of three OccD subfamily members whose crystal structures have been determined recently [9]. These are OccD1, OccD2, and OccD3. On the molecular surface representation, the side chains of positive residues are colored blue and those of negative residues are marked in red. On the ribbon representation, the bulkier, constriction-forming loops, including loops L3, L4 and L7, are colored green, yellow and orange, respectively. All the charges are estimated at pH=7.4; (**B**) Side view of the OccD1, OccD2, and OccD3 channels in a planar lipid bilayer. The charged amino acids are colored as described above. The vertical sticks represent the lipid molecules of the bilayer; (**C**) The top-to-bottom view of OccD3 channel with (left) and without (right) N-terminus. The N-terminus is 30-residue long. It contains two positive and two negative charges (PAPDNPSYAAEVQSIPSVAKPIKGQAGATG). Here, top is the extracellular side, so the N terminal is located within the extracellular side.

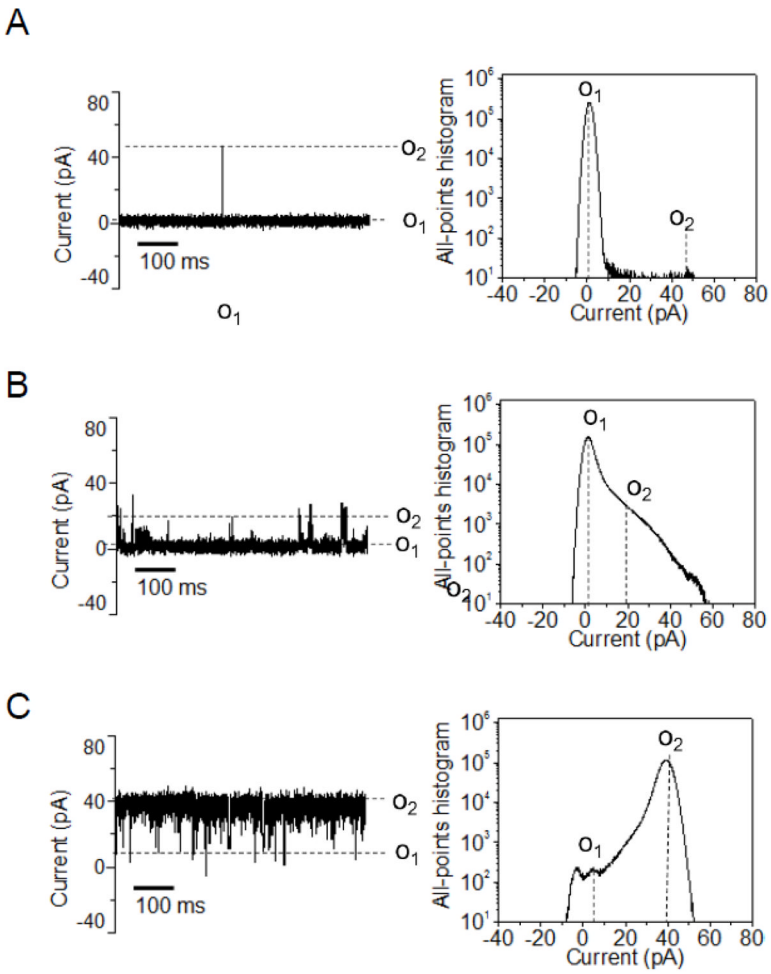

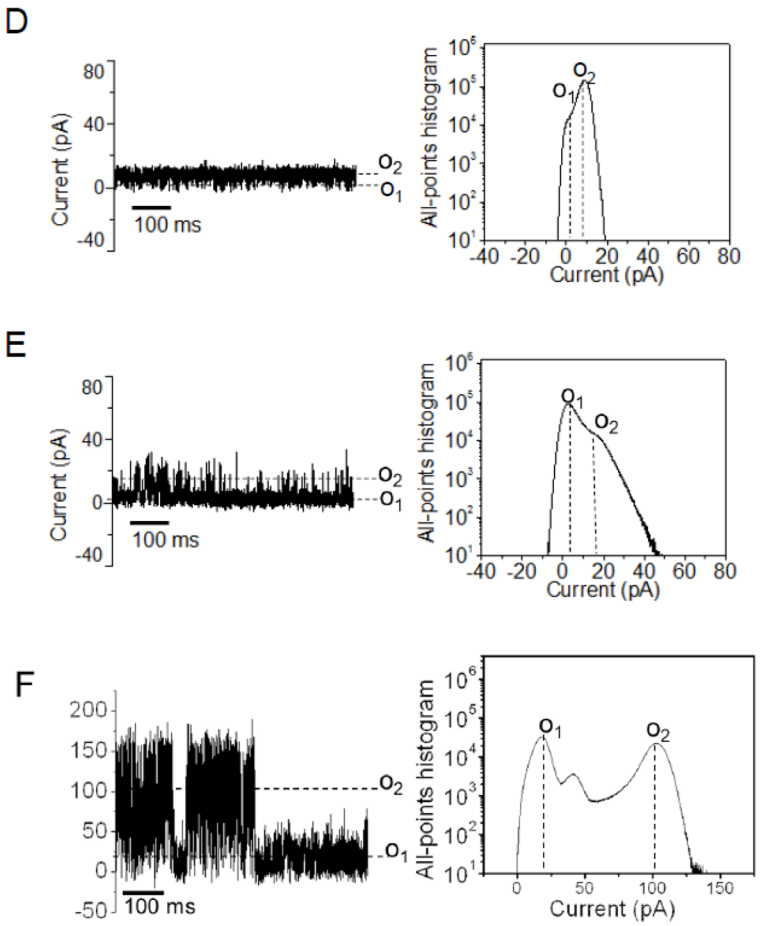

Figure 2. Typical single-channel electrical traces of six members of the OccD subfamily and their corresponding all-points current amplitude histograms

The single-channel electrical traces were recorded at a transmembrane potential of +60mV. The buffer solution was 1M KCl, 10 mM potassium phosphate, pH 7.4. (**A**) OccD1, (**B**) OccD2, (**C**) OccD3, (**D**) OccD4, (**E**) OccD5 and (**F**) OccD6. Current levels were marked both on the single-channel electrical traces and on the all-points current amplitude histograms. All single-channel electrical traces were low-pass Bessel filtered at 2 kHz. The "*" is indicated for the OccD2 channel, whose baseline of the O_1 open sub-state varied between 2 and 17 pA. All electrical traces were representative over at least three independent single-channel electrical recordings.

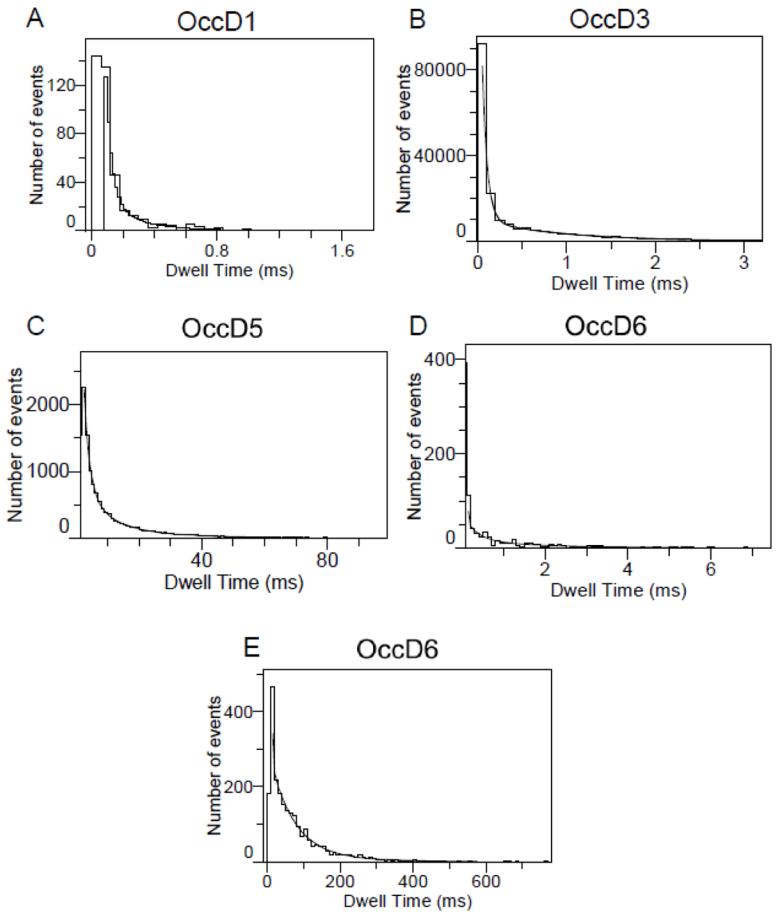

Figure 3.

Standard dwell-time histograms of representative single-channel electrical traces fitted with exponential probability functions. Each of these histograms are only representative to one single-channel recording as the dwell time analysis across different experiments is not possible due to large variation of the dwell time behavior. OccD2 and OccD4 exhibited irresolvable dwell times. The fits were based upon log likelihood ratio (LLR) tests with a given confidence level of 0.95 [s27; 54; 55]. The results of the fits were the following: (**A**) OccD1, $\tau_{O2} = 0.11 \pm 0.02$ ms; (**B**) OccD3, $\tau_{O1\text{-}1} = 0.06 \pm 0.01$ ms and $\tau_{O1\text{-}2} = 0.92 \pm 0.04$ ms; (**C**) OccD5, $\tau_{O2\text{-}1} = 4.2 \pm 0.3$ ms, $\tau_{O2\text{-}2} = 15.3 \pm 0.7$ ms; (**D**) OccD6 $\tau_{O1\text{-}1} = 0.12 \pm 0.01$ ms and $\tau_{O1\text{-}2} = 1.9 \pm 0.2$ ms. OccD6 has two major open sub-states $O_1$and O_2. The O_2 open sub-state featured downward current spikes to the O_1 open sub-state; (**E**) OccD6, $\tau_{O2\text{-}1} = 4.6 \pm 0.5$ ms, $\tau_{O2\text{-}2} = 81.5$ ms ± 3.8 ms. The OccD2 channel exhibited irresolvable current sub-states. OccD4 also showed very low-amplitude, short-lived and irresolvable current spikes.

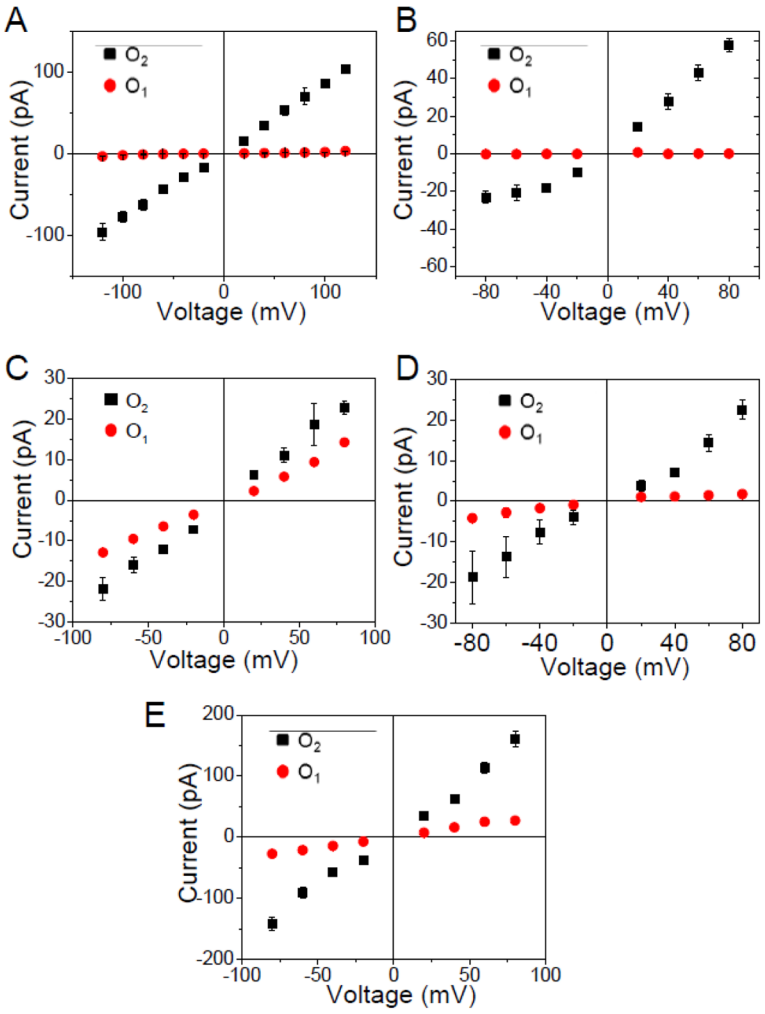

Figure 4. Current – voltage (I/V) profiles of all sub-states of the members of the OccD subfamily

(**A**) OccD1; (**B**) OccD3; (**C**) OccD4; (**D**) OccD5 and (**E**) OccD6. The data shown in these panels represents the average of at least three independent experiments. The lack of some data points is due to the low frequency and/or amplitude of these flickering events at a low applied transmembrane potential. OccD2 data is not shown owing to the large variability in the baseline of O_1 and O_2 open sub-states. The buffer solution was 1M KCl, 10 mM potassium phosphate, pH 7.4.

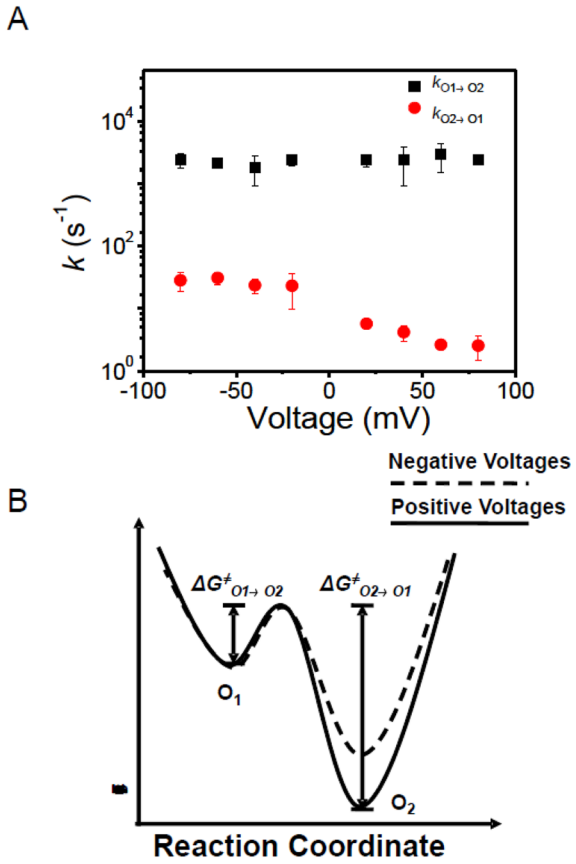

Figure 5. Single-channel event kinetics of the OccD3 channel

(**A**) voltage dependence of the kinetic rate constants; (**B**) free energy landscape model of the OccD3 channel. The significant voltage-dependence of the transition rates between O_1 and O_2 open sub-states suggested that the height of free energy barrier reduces when switching the applied transmembrane potential from positive to negative values.

Table 1

Ion selectivity values and conductance asymmetry ratios of the OccD proteins. [a]

g_{O1} and g_{O2} represent single-channel conductance values corresponding to the open sub-states O_1 and O_2, respectively. The single-channel conductance that corresponds to the most probable open sub-state is shown in bold. These parameters were calculated using a transmembrane applied potential of +60 mV. *g*'s were given in pS. The asymmetry conductance ratios of the most probable sub-state (g_{80}/g_{-80}) at +80 mV to that at −80 mV were determined in 1M KCl, 10 mM potassium phosphate, pH=7.4. The reversal potential (V_r) is the applied transmembrane potential that offsets the resting potential of the channel under KCl concentration gradient conditions. The reversal potential values were measured when the concentrations of KCl in *cis* and *trans* were 0.2 M and 1M, respectively, under similar conditions of buffer and pH (10 mM potassium phosphate, pH=7.4). Permeability ratios (P_k/P_{Cl}) were calculated based upon the reversal potential V_r, as discussed in the main text [31; 32; 49]. The reversal potential of the OccD1 and OccD2 channels were determined by eliminating the high-conductance state.

Protein	g_{01} (pS)	g_{02} (pS)	g_{80}/g_{-80}	V_r (mV)	P_k/P_{Cl}	Selectivity
OccD1	**21 ± 3**	889 ± 102	2.58 ± 0.97	−15 ± 7	2.5 ± 1.0	Cation-selective
OccD2	NA[b]	NA[b]	0.99 ± 0.30	−20 ± 8	3.5 ± 1.5	Cation-selective
OccD3	3.0 ± 3.0	**667 ± 71**	2.55 ± 0.26	−18 ± 1	3.0 ± 0.2	Cation-selective
OccD4	3.0 ± 0.1	**159 ± 8**	1.11 ± 0.08	−20 ± 2	3.5 ± 0.5	Cation-selective
OccD5	**24 ± 11**	239 ± 34	0.42 ± 0.08	−32 ± 3	12 ± 4	Cation-selective
OccD6	**417 ± 117**	1889 ± 151	0.99 ± 0.16	−24 ± 4	5.0 ± 1.4	Cation-selective

[a] The crystal structures of the OccD4, OccD5 and OccD6 proteins are not available.

[b] The baseline that corresponds to the O_1 open sub-state in various single-channel experiments varied between 2 and 17 pA when the applied transmembrane potential of +60 mV. Therefore, were not able to determine these values with satisfactory accuracy.

Table 2

The determination of the diameter and the charges near constriction for the OccD channels

The diameter of the OccD3 channel in the central constriction was determined using the HOLE software program [50–52] and its high-resolution crystal structure [9]. The number of the charged residues in the central constriction of the OccD3 channel were found using the PyMol and Chimera software programs [53]. The crystal structures of the OccD4, OccD5 and OccD6 proteins are not available.

Protein	Diameter (Å)	Charges located near the constriction
OccD1[a]	< 3	N/A[b]
OccD2[a]	< 3	N/A[b]
OccD3	~3.5	(−) D11, E18, D171, D342 (+) K27

[a]The diameters of the central constriction of the OccD1 and OccD2 channels were not determined, because they are too small. For example, using the HOLE program we were able to determine negative values for the diameters of the OccD1 and OccD2 central constrictions, in accord with the recent crystallographic study that showed OccD2 as a closed channel [9].

[b]The charges located within the central constriction of the OccD1 and OccD2 channels cannot be resolved with a satisfactory precision owing to the small size and the non–uniform orientation of the central eyelet of the channel.